Journal of Structural Biology: X 6 (2022) 100056

Contents lists available at ScienceDirect

Journal of Structural Biology: X

journal homepage: www.sciencedirect.com/journal/journal-of-structural-biology-x

Multimodal imaging reveals membrane skeleton reorganisation during reticulocyte maturation and differences in dimple and rim regions of mature erythrocytes

Adam J. Blanch [a], Juan Nunez-Iglesias [a,b], Arman Namvar [a,c], Sebastien Menant [d], Oliver Looker [a], Vijay Rajagopal [c], Wai-Hong Tham [d,e], Leann Tilley [a,1,*], Matthew W. A. Dixon [d,f,1,*]

[a] Department of Biochemistry and Molecular Biology, Bio21 Institute, University of Melbourne, Melbourne, Australia
[b] Monash University, Melbourne, Australia
[c] Department of Biomedical Engineering, University of Melbourne, Melbourne, Australia
[d] Division of Infectious Diseases and Immune Defence, The Walter & Eliza Hall Institute, Melbourne, Australia
[e] Department of Medical Biology, University of Melbourne, Melbourne, Australia
[f] Department of Infectious Diseases, The Peter Doherty Institute, University of Melbourne, Melbourne, Australia

ARTICLE INFO

Edited by ED-Bauke W. Dijkstra

Keywords:
Reticulocyte
Erythrocyte
Membrane skeleton
Shape memory
SEM
AFM

ABSTRACT

The red blood cell (RBC) is remarkable in its ability to deform as it passages through the vasculature. Its deformability derives from a spectrin-actin protein network that supports the cell membrane and provides strength and flexibility, however questions remain regarding the assembly and maintenance of the skeletal network. Using scanning electron microscopy (SEM) and atomic force microscopy (AFM) we have examined the nanoscale architecture of the cytoplasmic side of membrane discs prepared from reticulocytes and mature RBCs. Immunofluorescence microscopy was used to probe the distribution of spectrin and other membrane skeleton proteins. We found that the cell surface area decreases by up to 30% and the spectrin-actin network increases in density by approximately 20% as the reticulocyte matures. By contrast, the inter-junctional distance and junctional density increase only by 3–4% and 5–9%, respectively. This suggests that the maturation-associated reduction in surface area is accompanied by an increase in spectrin self-association to form higher order oligomers. We also examined the mature RBC membrane in the edge (rim) and face (dimple) regions of mature RBCs and found the rim contains about 1.5% more junctional complexes compared to the dimple region. A 2% increase in band 4.1 density in the rim supports these structural measurements.

Introduction

The human RBC is one of the simplest cell types, comprising of a lipid bilayer and an underlying spectrin-actin protein network, which are connected through integral membrane proteins. During its ~120-day life span, the disc-shaped human RBC requires a high level of deformability and durability as it circulates approximately a million times, squeezing through narrow capillaries and the 1–2 μm inter-endothelial slits that separate the splenic cords and venous sinuses (An and Mohandas, 2008).

The viscoelasticity of the RBC plasma membrane is thought to derive from its sub-membranous protein meshwork (Mohandas and Gallagher, 2008). Although well studied, the structure of the membrane protein network is still not fully elucidated (Lux, 2016). The junctional complexes comprise many interacting proteins in arrangements that depend on dynamic exchange processes and levels of phosphorylation. This makes accurately defining the architecture of the membrane skeleton and the distribution of proteins within this network challenging. Proteomics studies are helping to understand the composition of membrane network proteins (Basu et al., 2015), while the resolving power of

* Corresponding authors at: Department of Infectious Diseases, The Peter Doherty Institute, University of Melbourne, Melbourne, Australia (M.W.A. Dixon) and Department of Biochemistry and Molecular Biology, Bio21 Institute, University of Melbourne, Melbourne, Australia (L. Tilley).
E-mail addresses: ltilley@unimelb.edu.au (L. Tilley), matthew.dixon@unimelb.edu.au (M.W.A. Dixon).
[1] Equal senior authors.

https://doi.org/10.1016/j.yjsbx.2021.100056
Received 30 August 2021; Received in revised form 18 November 2021; Accepted 4 December 2021
Available online 8 December 2021

structural imaging techniques continues to improve (Nans et al., 2011).

It has previously been established that the core component of the protein mesh is an array of spectrin heterodimers that self-associate head-to-head to form tetramers. The tails of the spectrin heterodimers are linked into junctional complexes containing actin oligomers (each with 14–16 protomers), protein 4.1R, adducin and additional accessory proteins (Fowler, 2013; Mankelow et al., 2012; Salomao et al., 2008). Flexible linkages between the triple-helical segments of the spectrin heterodimers, spectrin tetramer dissociation and breakable linkages at the junction points are thought to accommodate the shear forces imposed on the RBC during circulation. Vertical interactions connect the skeletal meshwork to the plasma membrane. A sub-population of band 3 dimers are connected to spectrin via ankyrin, while the remaining population of band 3 dimers participate in a glycophorin C/protein 4.1 interactions and band 3/adducin interaction (Fowler, 2013; Mankelow et al., 2012).

Reticulocyte maturation is the final step of terminal erythroid differentiation, and reticulocytes typically compose about 1% of the RBCs in circulating peripheral blood. Multilobular reticulocytes develop and mature in the bone marrow and then circulate for about a day in the blood stream before developing into mature discoid RBCs. During this process, membrane vesiculation leads to loss of approximately 20% of the RBC surface area (Come et al., 1972; Gifford et al., 2006; Waugh et al., 1997), and the plasma membrane becomes more stable and more elastic (Chasis et al., 1989; Waugh et al., 2001). These changes imply reorganisation of the membrane bilayer, the skeletal components and the vertical linkages; however, only a few studies have attempted to measure the reorganisation directly (Gautier et al., 2018; Li et al., 2018; Liu et al., 2010; Minetti et al., 2018; Ovchynnikova et al., 2018). Understanding the reorganisation of the membrane skeleton during reticulocyte maturation is crucial to understanding the remarkable biomechanical properties of mature RBCs.

Mature RBCs have been reported to exhibit shape memory (Fischer, 2004), and to orient themselves preferentially within a centrifugal field (Hoffman, 2016; Hoffman, 2018). These previous studies suggest a structural difference between the rim (edge) and dimple (face) of the RBC biconcave disc. Non-muscle myosin IIA (NMIIA) is proposed to play a role in generating tension in skeletal network and thus maintaining RBC shape, forming bipolar filaments that associate with F-actin oligomers in junctional complexes (Smith et al., 2018). NMIIA is reported to have a higher concentration in the RBC dimple region than at the rim (Alimohamadi et al., 2020); however, direct measurement of the membrane network density at the rim and edge has not been performed.

Here we investigate differences in membrane skeleton organisation between CD71 (otherwise known as transferrin receptor, TfR)-expressing reticulocytes and mature RBCs, as well as between the edge and dimple regions of mature RBCs. Differences were assessed using fluorescence-based analysis of immuno-labelled structural proteins, combined with ultrastructural measurements taken from SEM and AFM images of the cytosolic surface of the protein network.

Methods

Materials

Human O+ red blood cells (RBCs) were provided by the Australian Red Cross Blood service. Erythroagglutinating lectin from red kidney bean (*Phaseolus vulgaris;* phytohemagglutinin (PHA-E)) was obtained as lyophilized powder from Sigma Aldrich and dissolved in PBS. Glutaraldehyde (Grade I, 25% in H_2O), (3-Aminopropyl)triethoxysilane (APTES), EPB41 rabbit antibody (HPA028414) and DMTN rabbit antibody (HPA024290) were also purchased from Sigma-Aldrich. Bis(sulfosuccinimidyl)suberate (BS3), Alexa 488 anti-mouse/rabbit, Alexa 568 anti-mouse, Alexa 647 anti-mouse/rabbit, Ankyrin 1 mouse antibody (S388A-10) and FITC-conjugated TfR/CD71 monoclonal antibody (MEM-75, MA1-19577) were obtained from Life Technologies (Thermo Fisher). Anti-CR1/CD35 (ab25, ab76520) and anti-TfR/CD71 (ab38171) antibodies were obtained from Abcam. The pre-conjugated antibody to CD71 was used in shearing experiments to prevent aggregate formation when using secondary labels.

Purification of reticulocytes

500 mL of whole peripheral blood (Australian Red Cross) or 70–100 mL cord blood (BMDI Cord Blood Bank) was passed through a RC high efficiency leucocyte removal filter (Haemonetics, Australia) and washed three times with PBS to remove the serum component. RBCs at approximately 50% haematocrit were layered onto a 70% (v/v) isotonic Percoll cushion (GE Healthcare) and centrifuged for 25 min at 2000 × g. The thin band formed at the Percoll interface was collected as the reticulocyte fraction, while the pellet was collected as the mature cell fraction. In some samples, a second Percoll separation was performed to increase the reticulocyte percentage. Cells were stored in RPMI wash buffer (Gibco) at 4 °C until further usage.

For three peripheral blood repeats, reticulocytes were enriched by passing cells labelled with magnetic micro beads targeting CD71 (Miltenyi Biotec, 130-046-201) through a magnetic column and eluting the trapped cells. The CD71+ population was measured as >82% in each enriched sample.

For all other repeats, mature RBCs and reticulocytes were mixed at a ratio of 1:3 following differential labelling before HEMA or immunofluorescence measurements. Unlabelled cells were considered to be CD71- reticulocytes, however this fraction also includes unlabelled (CD35-) mature cells.

Preparation of differentially labelled whole cells

Whole RBCs or separated reticulocytes were washed in PBS before addition of primary antibodies at 1:250 (CR1) or 1:500 (CD71) in PBS with 3% BSA for 1 hr at room temperature (RT). Cells were further incubated with Alexa fluor 488 or 568 secondary antibodies in PBS with 3% BSA at 1:500 for 1hr at RT as required. Membranes were rinsed 3 times with PBS after addition of both primary and secondary reagents.

Preparation of sheared membranes

Coverslips (25 mm, or 12 mm for AFM) were scored with a diamond tip pen to create markers for correlative imaging, washed in acetone and then 50% methanol in water for 5 mins each, then air dried. Dry coverslips were immersed in a mixture of 28 mL acetone, 1.5 mL water and 0.6 mL APTES for 3 min. Coverslips were further washed in acetone (2x), water and PBS for 5 mins each before transfer to humidified containers. 0.5 mg/mL BS3 in PBS was applied to the surfaces for 30 min and rinsed off. Surfaces modified with PHA-E and poly-L-lysine were prepared by immersing BS3 coated surfaces in 0.1 mg/mL solutions of the protein/polymer in PBS for 2 h at RT. Free binding groups from BS3 were quenched by 30 min incubation with 0.1 M glycine in PBS before final rinsing and storage in PBS. Coverslips were used immediately for best results, however PHA-E coverslips could be stored in PBS at 4 °C for up to 10 days.

RBCs at 1–2% haematocrit in PBS were washed twice in PBS before addition to the coverslip surface. Binding was performed at RT for 1 hr. Excess free RBCs were rinsed off before bound RBCs were sheared by applying a continuous jet of 5P8-10 buffer (5 mM Na_2HPO_4/NaH_2PO_4, 10 mM NaCl, pH 8) from a 30 mL syringe (23-G needle) at an angle of ~20°. Sheared membranes were fixed immediately following shearing; 4% paraformaldehyde and 0.0065% glutaraldehyde in PBS was applied for 20 mins at RT prior to immunostaining.

Preparation of membranes at different osmolality

The PBS buffer osmolarity was tuned by adjusting the NaCl

concentration of the medium from 137 mM (physiological) to 111 mM (hypotonic) while keeping the Na_2HPO_4, KH_2PO_4 and KCl concentrations constant at 10, 1.8 and 2.7 mM respectively, and the pH was adjusted to 7.35 with small volumes of 2 M HCl. Osmolarity was measured as 140 mOsm/kg and 288 mOsm/kg for hypotonic and physiological conditions, respectively, using an Advanced Instruments 3320 freezing-point osmometer.

Labelled RBCs in physiological buffer were adhered to a PHA-E coated coverslip for 2 min. Excess cells were removed by rinsing with physiological buffer and bound cells were incubated for 30 min before exchanging the buffer to hypotonic PBS. Counter-labelled RBCs were redispersed in hypotonic PBS and incubated on the same coverslip for 30 mins. Cells were then rinsed with 1X PBS, reference images taken, and shearing with 5P8-10 performed.

Preparation of edge orientated membranes

Prior to orientation experiments RBCs were incubated in RPMI media at 37°C for at least 2 hr and then washed twice in PBS before immediate use. 0.6 mL of 8 mg/mL 360 kDa PVP was placed on a clean coverslip with a 20 mm diameter o-ring. 50 μL of RBC in PBS was mixed in with a pipette and roleaux were allowed to form for 10 min. A PHA-E coated slide (from which excess PBS was wicked off) was placed on top of the o-ring and the sandwich structure was inverted, allowing pre-formed roleaux to settle onto the PHA-E under gravity. After 20 mins the coverslip was rinsed and allowed to stand for a further 40 mins in PBS before imaging, shearing or preparation for whole-cell SEM. Note that casein was also trialled as an agglutinating agent and was found to block RBC binding to PHA-E.

Immunostaining and fluorescence microscopy

Sheared membranes were blocked with 3% bovine serum albumin in PBS for 30 mins before incubation with primary antibodies. Actin was detected using phalloidin conjugated to Alexa-647. Ankyrin was targeted with a monoclonal antibody, while other proteins were detected using polyclonal rabbit antibodies. Primary antibodies were added at 1:250 or 1:500 in PBS with 3% BSA for 1 hr at room temperature. Membranes were further incubated with Alexa fluor 647 secondary antibody in PBS with 3% BSA at 1:500 for 1hr. Membranes were rinsed with 2–3 mL of PBS after addition of both primary and secondary reagents before imaging. Samples were imaged on a DeltaVision Elite Widefield Imaging System (GE Healthcare). Excitation was achieved with solid state illumination (Insight SSI, Lumencor). The following filter sets with excitation and emission wavelengths were used: FITC, Ex475/28, Em523/26; TRITC, Ex542/27, Em594/45; Cy5 Ex 632/22, 676/34 nm, in combination with a 100x UPLS Apo (Olympus, 1.4 NA) oil immersion objective lens.

For intensity measurements, dark-field and flat-field corrections were applied using correction images collected at the same time as the data sets. Image intensity per area was measured using ROIs 40 × 40 pixels wide at the centre of sheared membranes. For the edge-oriented cells and comparative face-on cells in the same images, 4 separate 16 × 16 pixel ROIs were defined on each membrane as close as possible to the centre and the mean was taken.

Microfluidics measurements

A highly diluted (~0.2% haematocrit) mixture of labelled reticulocytes and mature RBCs was passed into a microfluidics device (HEMA) (Gifford et al., 2006; Namvar et al., 2021) at a flow pressure of 180–250 Pa using an Elveflow AF1 pressure pump. Microfluidic chips were mounted in the DeltaVision Elite microscope and imaged using a 40x air objective at RT. Images were collected in brightfield as well as red, green and blue fluorescence channels to facilitate identification of cell populations as well as automated analysis using the shadow of RBC haemoglobin. Acquired images were analysed in ImageJ (NIH Image/ImageJ) and cells were delineated automatically using a macro plugin developed in-house. Volume and surface area were calculated by importing the measurements into R software.

Scanning electron microscopy (SEM)

Whole RBC cell samples bound to glass coverslips were immersed in 0.05% glutaraldehyde in PBS for 20 min prior to final fixation to prevent osmotic shock. Final fixation of whole cells and sheared membranes before SEM/AFM was performed using 2.5% glutaraldehyde in PBS for 2 h at RT.

After transfer from fixative to H_2O, fixed, hydrated samples were sequentially transferred to mixtures of 20, 50, 70, 80, 90, 95 and (3x) 100% ethanol in H_2O for 5 min each before transfer into a Leica CPD300 critical point dryer, which was run with a minimum of 12 exchange cycles into liquid CO_2.

Dehydrated coverslips with attached membranes were gold coated to a thickness of 0.4 nm using a current of 10 mA in a Safematic CCU-010 sputter coating system. Alternatively, whole cell sputter coating was carried out on the rotating mount of a Dynavac SC100 sputter coating instrument for 75 s using a 25 mA current.

Images were acquired with the ETD detector of an FEI Teneo SEM in Optiplan mode, at a working distance of 5 mm, with a beam current of 50 pA and a 2 kV accelerating voltage. Images for *skan* analyses were collected at 200–250 000 × magnification with 1536 × 1024 pixels.

Atomic force microscopy (AFM)

Images were acquired on an Asylum Research Cypher ES instrument in tapping mode. Silicon nitride BL-AC40TS probes were driven at their nominal frequency (approximately 25 kHz) using the blue drive photothermal excitation system for fluid imaging. Images analysed by *skan* software were acquired at 512 × 512 pixels at 2 Hz or 1024 × 1024 pixels at 0.5 Hz using a scan angle of 90°. Images were levelled using mean plane subtraction and corrected for horizontal strokes using Gwyddion software. A median filter (3 pixel radius) was applied to remove spikes from tip-sample adhesion before *skan* analysis.

Tracing networks automatically using skan

Images of membrane networks were processed using the python package *skan* (Nunez-Iglesias et al., 2018) to extract values for branch length, branch density, junction density, and mesh area, and data points presented in scatter plots are the mean per image (for AFM and edge/face datasets) or grouped by cell mean (i.e. multiple images per cell; control, osmolarity and reticulocyte datasets) from SEM data. Results presented for mean branch length include only junction to junction branches and were filtered for shape index between 0.125 and 0.625 (ridges only). For SEM measurements in the reticulocyte experiments, the mesh area measurement was modified to include meshes touching the boundary to remove bias in networks with large meshes. Other comparisons exclude incomplete meshes. *Skan* parameters were set to use Gaussian smoothing with a radius of 0.1x the thresholding radius. The threshold radius was set to 50 nm with a brightness offset of 0 for SEM data, while for AFM data these values were adjusted to a threshold radius of 25 nm, with an offset of 0.05. These values were tested and found far more likely to miss branches in the image rather than introduce false branches into the trace. It is therefore likely that our measurements slightly under-represent the connectivity and density of the true membrane networks.

Statistics

Data from separate populations was compared using an unpaired, two-tailed *t*-test. Significance is indicated in distribution plots by

asterisks in the figures, where * = $p < 0.05$, ** = $p < 0.01$, *** = $p < 0.001$. Those with p values > 0.05 are not significant (ns).

Results

Low variance in fluorescence signal and SEM membrane skeleton measurements from control samples validates the microscopy-based approaches

In order to determine if we could accurately measure changes in membrane architecture and protein densities within RBC membranes, we developed a set of criteria to ensure accurate comparison between samples and cell types. We contend that different cell types being compared should be processed and imaged in the same sample (if possible) and within the same field of view. We validated the method using two mature RBC samples from the same source labelled with a primary antibody to the RBC surface protein, Complement Receptor 1 (CR1), and secondary antibodies conjugated to Alexa 568 and Alexa 647 fluorophores. The two samples were mixed after differential labelling and adhered to coverslips coated with the RBC-binding lectin, phytohemagglutinin (PHA-E)), prior to being hypotonically sheared as previously described (Looker et al., 2019). The cytoplasmic surface was labelled with antibodies recognising either anti-spectrin or anti-band 4.1, and prepared for fluorescence imaging (Fig. 1a and S1a) (Looker et al., 2019). No statistically significant difference was observed between the fluorescence intensities of spectrin (Fig. 1b) or band 4.1 (Fig. S1b) labelling within the two CR1-labelled populations.

For further evaluation, differentially labelled whole RBCs were prepared as above and attached to marked coverslips. Reference fluorescence images for identifying sub-populations were recorded from whole cells before sheared membranes were prepared. The membranes were fixed and dehydrated and SEM was used to image the membrane skeleton network. SEM images were analysed using a custom-built python program called *skan* (Nunez-Iglesias et al., 2018). Skan returns statistics for the parameters of mean branch length, branch density per unit area, mean junctions per unit area (i.e. 2 or more branches connecting), and mean mesh area for each image examined (Fig. S2). We saw no statistical differences in the mean branch lengths of the two differentially labelled populations (Fig. 1c–e), suggesting that inherent variation in the measurements is low.

Osmotic swelling leads to discernible changes in RBC membrane structure and protein density

We applied our imaging techniques to measure the membrane skeleton structure and protein densities in cells which were artificially expanded using hypotonic buffer. RBCs from the same batch of blood were differentially labelled as described above and then incubated in low osmolarity conditions (140 mOsm/kg) to swell the cell or in physiological conditions (288 mOsm/kg) prior to and during attachment to the glass surface. Sheared membranes were labelled with anti-band 4.1 or anti-spectrin antibodies (Fig. 2a, c). Two repeats of the fluorescence intensity measurements were performed. Osmotically swollen RBCs exhibited a 5.4% ± 2.8% reduction in fluorescence signal per unit area for spectrin, and band 4.1 showed a 3.2% ± 3% decrease upon swelling. Representative data is shown in Fig. 2b (band 4.1) and Fig. 2d (spectrin).

We next assessed the physical changes to the membrane skeleton (Fig. 2e, f). SEM imaging revealed that the branch length and the mean mesh area size increased by 3.5 ± 0.3% and ~7% respectively, while the branch density and junction density respectively decreased by 5.9 ± 4.9% and 6.5 ± 5.9% in osmotically swollen cells (means from 5 repeat experiments). Relative ratios (hypotonic/physiological) for network statistics from each individual repeat are shown in Fig. S3, with representative data in Fig. 2g–j. These data are consistent with the changes in the individual protein labelling profiles observed by immunofluorescence microscopy.

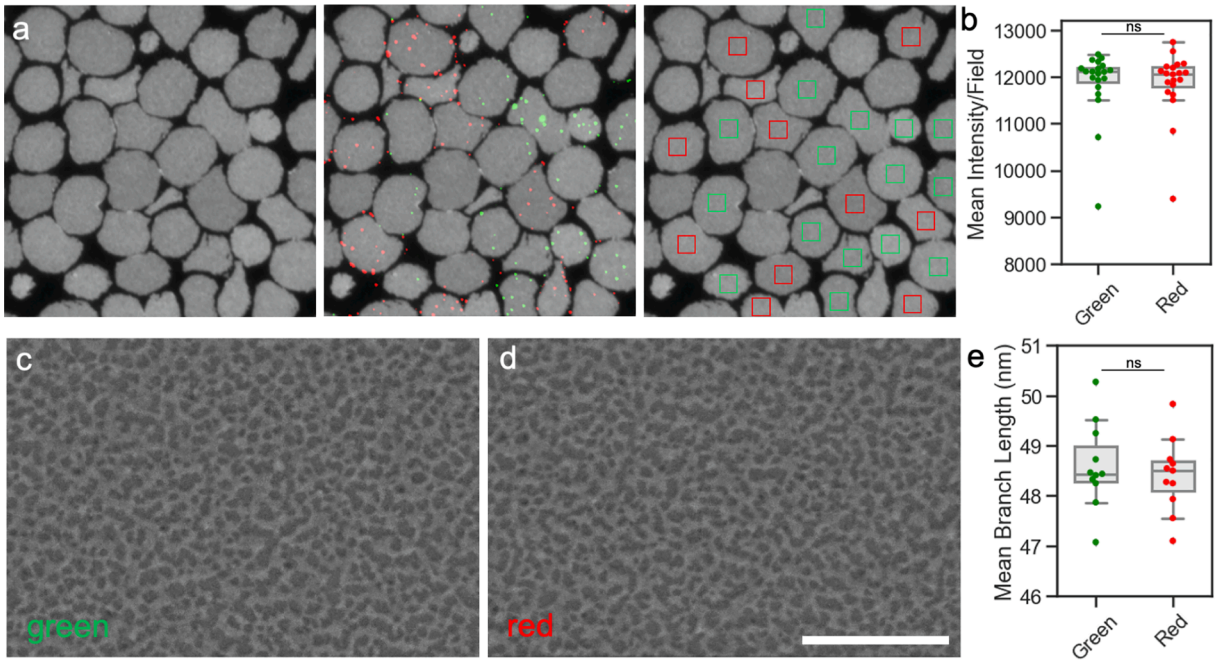

Fig. 1. Spectrin labelling and skeletal meshwork organisation are homogeneous across different cells. (a) RBCs were incubated with anti-CR1, and two separate populations were labelled with different Alexa-conjugated secondary antibodies (green and red). RBCs were adhered to glass coverslips and sheared. The remnant membrane disks were labelled with anti-spectrin antibodies (grey scale) and imaged (a partial 60X field is shown). The coloured squares identify the regions of the cells measured. (b) Mean areal intensity values for membrane discs in each field, from 20 fields each containing >20 cells per population. Unpaired T-test: not significant (ns) = $p > 0.05$. (c-d) Representative SEM images from sheared membranes of each population. (e) *Skan* analysis showing the mean branch length for the 2 populations (11 membranes per population, 6 SEM images per membrane). Unpaired T-test: not significant (ns) = $p > 0.05$. Scale bar is 500 nm. (For interpretation of the references to colour in this figure legend, the reader is referred to the web version of this article.)

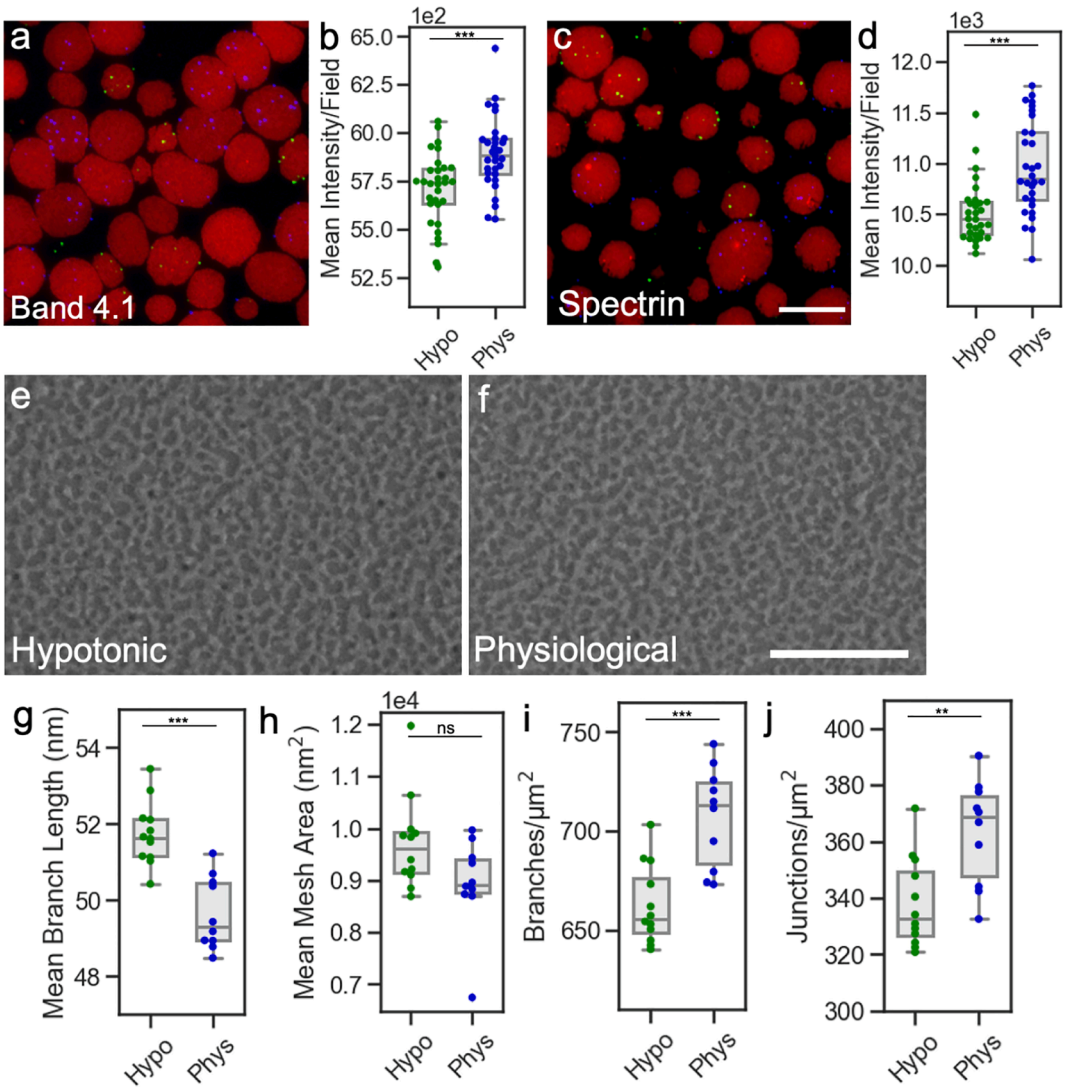

Fig. 2. Immunofluorescence and SEM analysis of sheared membranes from osmotically swollen RBCs. (a-d) RBCs labelled with CR1/Alexa 488 were surface bound under hypotonic conditions (140 mOsm/kg, shown as green), while RBCs labelled with CR1/Alexa 568 were maintained at physiological osmolarity (288 mOsm/kg, shown as blue) during attachment to glass coverslips. Sheared membranes were labelled with antibodies recognising band 4.1 (a, b) ($p = 0.0003$) or spectrin (c,d) ($p < 0.0001$) and Alexa 647 (red). Mean fluorescence intensity values are shown from at least 30 fields (min. 14 membranes per population per field). Scale bar = 10 µm, partial 60X field is shown. (e, f) SEM images of the protein network revealed increased membrane skeleton branch length (g) ($p < 0.0001$) and mean membrane skeleton mesh size (h) ($p = 0.0563$), along with decreased branch (i) ($p = 0.0002$) and junction (j) ($p = 0.0025$) densities in the hypotonic condition. SEM measurements were extracted from a minimum of 10 membranes per population, min. 5 images per membrane. Scale bar = 500 nm. (For interpretation of the references to colour in this figure legend, the reader is referred to the web version of this article.)

Surface area and volume are significantly decreased upon maturation of reticulocytes to mature cells

Reticulocytes, the earliest circulating form of RBC, can be separated from mature RBCs using density purification on a Percoll cushion. The reticulocyte population can be further divided into early reticulocytes, which are characterised by the expression of the surface marker CD71 (+), and mature reticulocytes that do not express CD71 (−). Using the differential staining method described above, Percoll-purified reticulocytes were labelled with anti-CD71 and Alexa 488 secondary antibodies, while the mature RBCs collected from the Percoll pellet were labelled with anti-CR1 and Alexa 568 secondary antibodies. The final mixed sample comprises three populations: CD71+ reticulocytes (Alexa 488), CD71- reticulocytes (no label) and CR1-labelled mature RBCs (Alexa 568).

We examined the volume and surface area of >200 cells using a purpose-built microfluidic device, the Human Erythrocyte Microchannel Analyser (HEMA) (Gifford et al., 2006; Namvar et al., 2021; Waugh et al., 1997). The volume and surface area of CD71- reticulocytes were 12% and 10% higher than mature RBCs, while the volume and surface area of CD71+ reticulocytes were 26% and 29% larger than mature cells, respectively (Fig. 3a, b). These measurements are consistent with previous results (Gifford et al., 2006; Namvar et al., 2021; Waugh et al., 1997).

Membrane protein density increases during maturation, while changes in the physical meshwork are less pronounced

CD71+, CD71- reticulocytes and mature RBCs were separated by Percoll density gradient and surface-labelled as described above. The cells were adhered to glass coverslips, sheared, then labelled with antibodies recognising six proteins known to be major components of the membrane protein network. The approximate physical locations of each structural protein are shown in the schematic (Fig. 3c). The fluorescence

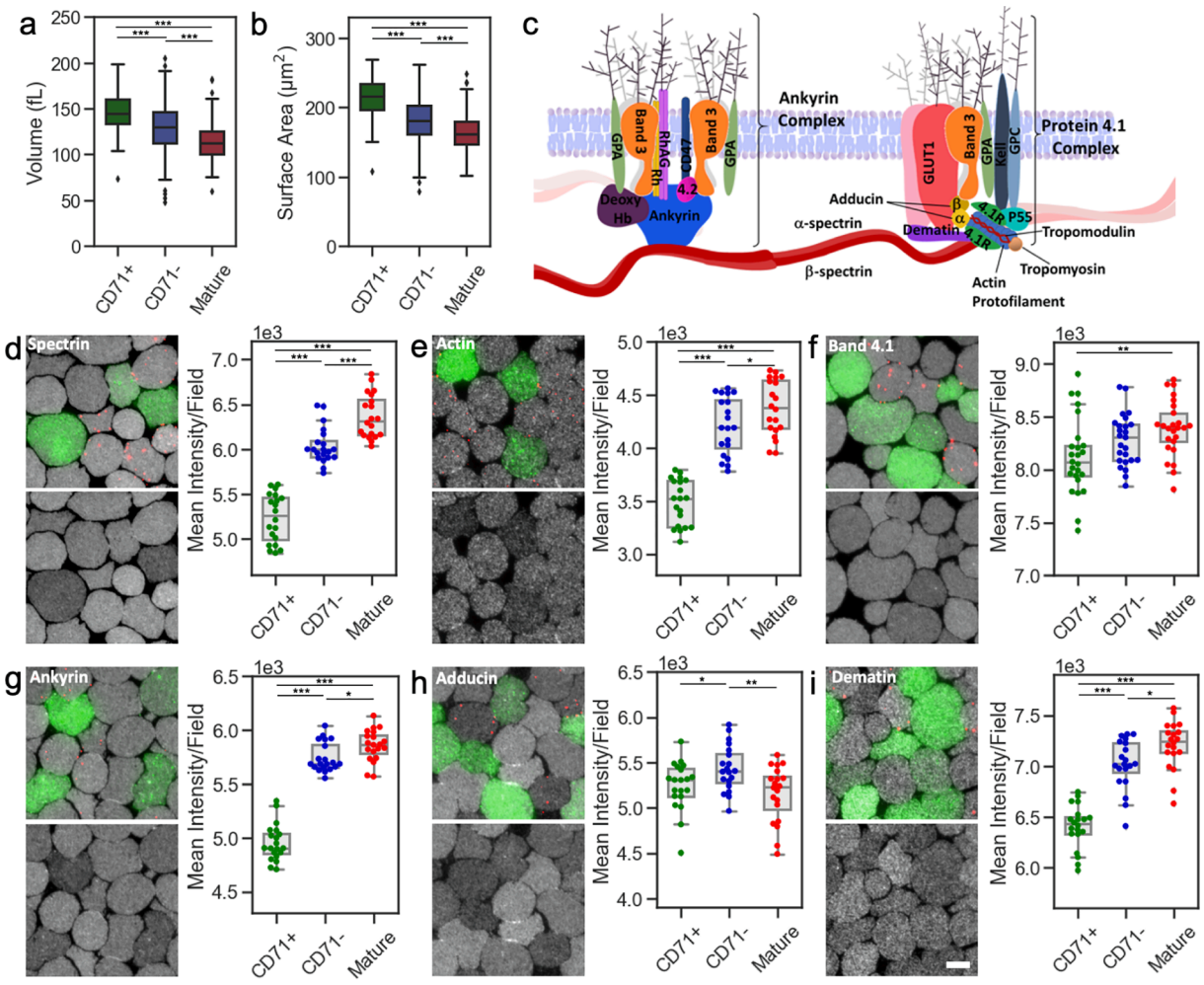

j

Protein	Spectrin	Band 4.1	Actin	Adducin	Ankyrin	Dematin
CD71-/Mature	0.95	0.99	0.96	1.08	0.98	0.97
SD	0.03	0.02	0.02	0.06	0.03	0.02
CD71+/Mature	0.84	0.94	0.79	1.03	0.85	0.86
SD	0.03	0.04	0.03	0.05	0.04	0.04
# of Repeats	5	4	4	3	3	3

Fig. 3. Loss of surface area as reticulocytes mature exceeds the loss of skeletal proteins. (a, b) HEMA analysis of volume and surface area for CD71+, CD71− reticulocytes and mature RBCs from the same sample. Unpaired T-test: *** = $p \leq 0.001$. (c) A schematic highlighting approximate protein positions within the junctional complexes. (d-i) Fluorescence intensity from sheared membranes stained with antisera against different membrane proteins. Representative images (partial fields) are shown for each protein, along with data for mean intensity values per full 60X field for each cell type. CD71+ cells are labelled and plotted in green, with mature cells labelled by CR1 plotted in red. CD71- cells are unlabelled and are plotted in blue, with membrane protein staining in greyscale. Scale bar = 5 μm. (j) Ratios of fluorescence intensities for CD71 + and CD71− reticulocytes relative to mature RBCs (means and standard deviations are shown, minimum of 10 image fields per repeat). Unpaired T-test: * = $p \leq 0.05$; ** = $p \leq 0.01$; *** = $p \leq 0.001$. (For interpretation of the references to colour in this figure legend, the reader is referred to the web version of this article.)

signal per unit area for actin was 21% higher in mature RBCs compared with CD71+ reticulocytes (Fig. 3e). The signals also increased for spectrin (16%, Fig. 3d), ankyrin (15%, Fig. 3g), dematin (14%, Fig. 3i) and Band 4.1 (6%, Fig. 3f). In contrast the fluorescence signal for adducin decreased slightly (3–4%, Fig. 3h). The ratios of fluorescence intensities for CD71+ and CD71− reticulocytes relative to mature RBCs are shown in Fig. 3j.

Next, image analysis of the RBC membrane skeleton was performed on samples imaged by correlative SEM (Fig. 4). Reticulocytes were prepared from different sources; three from peripheral blood, three from cord blood, and three from peripheral blood enriched using anti-CD71-tagged magnetic beads. In all cases the results were similar, with cord blood presenting marginally larger differences. SEM images of whole cells attached to PHA-E-coated coverslips and representative images of sheared membranes prepared from these cell types are shown for CD71+ (Fig. 4a, d), CD71− (Fig. 4b, e) and mature (Fig. 4c, f) cell types. Skan analysis of data for CD71+ (Fig. 4g) and CD71− (Fig. 4h) reticulocytes (9 separate experiments overall; 3 from each source type) reveals a 2.6% decrease in the branch length and 13.1% decrease in mesh area in mature RBCs compared with CD71+ reticulocytes, while the branch and junction density increased by 4.8% and 5.8% respectively. The change in branch length is mostly driven by a reduction in the total number of

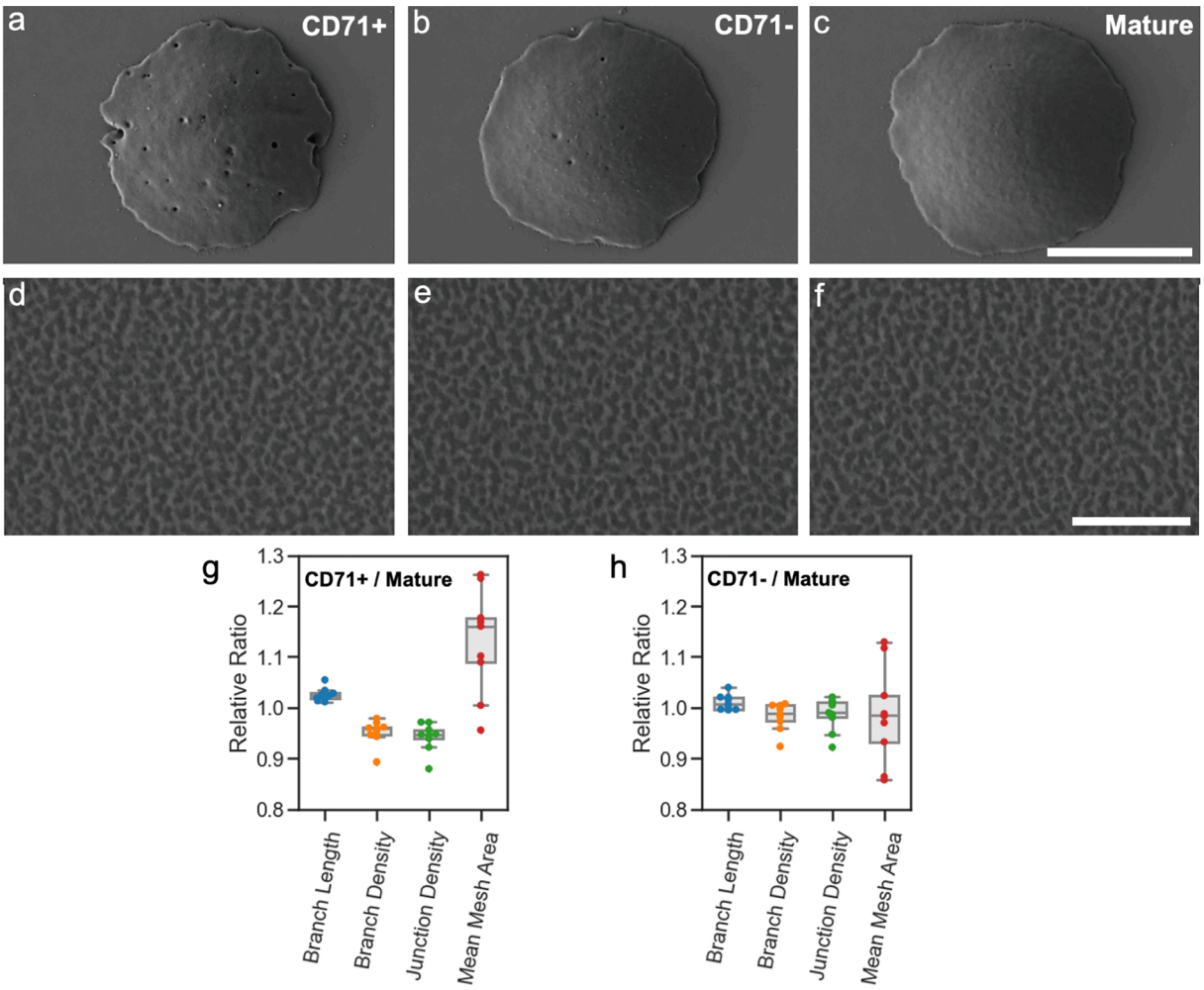

Fig. 4. Moderate shrinking of the physical skeletal meshwork is evident as reticulocytes mature. (a–c) SEM of whole cells and representative images of sheared membranes (d-f) for CD71+ (a,d) and CD71- (b,e) reticulocytes as well as mature RBCs (c,f) separated from peripheral blood and bound to PHA-E coated surfaces. Scale bars = 5 μm (a–c) and 500 nm (d–f). (g, h) *Skan* analysis was performed on sheared membrane networks from 9 independent experiments (3 cord blood, 3 peripheral blood, 3 magnetically enriched peripheral blood samples) with data for CD71+ (g) and CD71− (h) reticulocytes expressed as ratios of values obtained from mature RBCs within the same sample.

short branches in reticulocytes, as the distribution of branch lengths is not significantly shifted toward longer branch lengths. An example dataset from a single repeat is shown in Fig. S4 along with a histogram. We note that the adhesive molecule used to bind the RBCs to the glass slide before shearing can influence the organisation of the meshwork. We assessed reticulocyte membranes bound with both PHA-E and poly-l-lysine and found the same trends in both (Fig. S5).

Sheared membranes prepared from mature RBCs (Fig. 5a) and CD71+ reticulocytes (Fig. 5b) were fixed with glutaraldehyde and hydrated samples were examined using atomic force microscopy (AFM). 3 separate cord blood samples were examined, and 2 to 3 images were obtained for membranes of each cell type in each experiment. Meshwork analysis of the pooled samples using *skan* revealed a similar trend to the SEM analysis with a 4.1% and 18.3% decrease in branch length and mesh area for mature RBCs compared with reticulocytes (Fig. 5c, d), and an 8.1% and 9.1% increase in branch and junction density (Fig. 5e, f); however due to the small sample size of the AFM analysis statistical significance was not reached.

Fluorescence intensity and network measurements from SEM images show differences between the edge and face regions of the RBC

Samples containing edge-orientated and face-orientated RBC membranes were prepared using a method of rouleaux formation followed by attachment, hypotonic shearing and immunolabelling (Fig. 6a). No difference in the fluorescence signal per unit area was observed for the skeletal cross-member protein, spectrin (ratio edge : face 1.000 ± 0.016), while a slightly higher density of the junction protein, band 4.1 (ratio edge: face 1.021 ± 0.025) was observed at the edge. These ratios are the means of three individual repeats, with representative data shown in Fig. 6b and c for spectin and band 4.1 respectively.

SEM images of whole RBC rouleaux preparations as well as sheared membranes are presented in Fig. 6d–i. Analysis of the networks using *skan* shows a significant decrease in junction-junction branch length (edge: face ratio of 0.991) and mean mesh area (edge: face ratio of 0.949) for the edge-oriented membranes vs face-oriented membranes (Fig. 6j,k). In addition we also observe an increase in branch density (edge: face ratio of 1.014) and junction density (edge: face ratio of 1.012) when compared to the face-oriented membranes (Fig. 6l,m).

Discussion

Red blood cell membranes have previously been studied by TEM (Byers and Branton, 1985; Liu et al., 1987; Nans et al., 2011; Ohno, 1992; Ohno et al., 1994) and fluorescence microscopy (Pan et al., 2018)

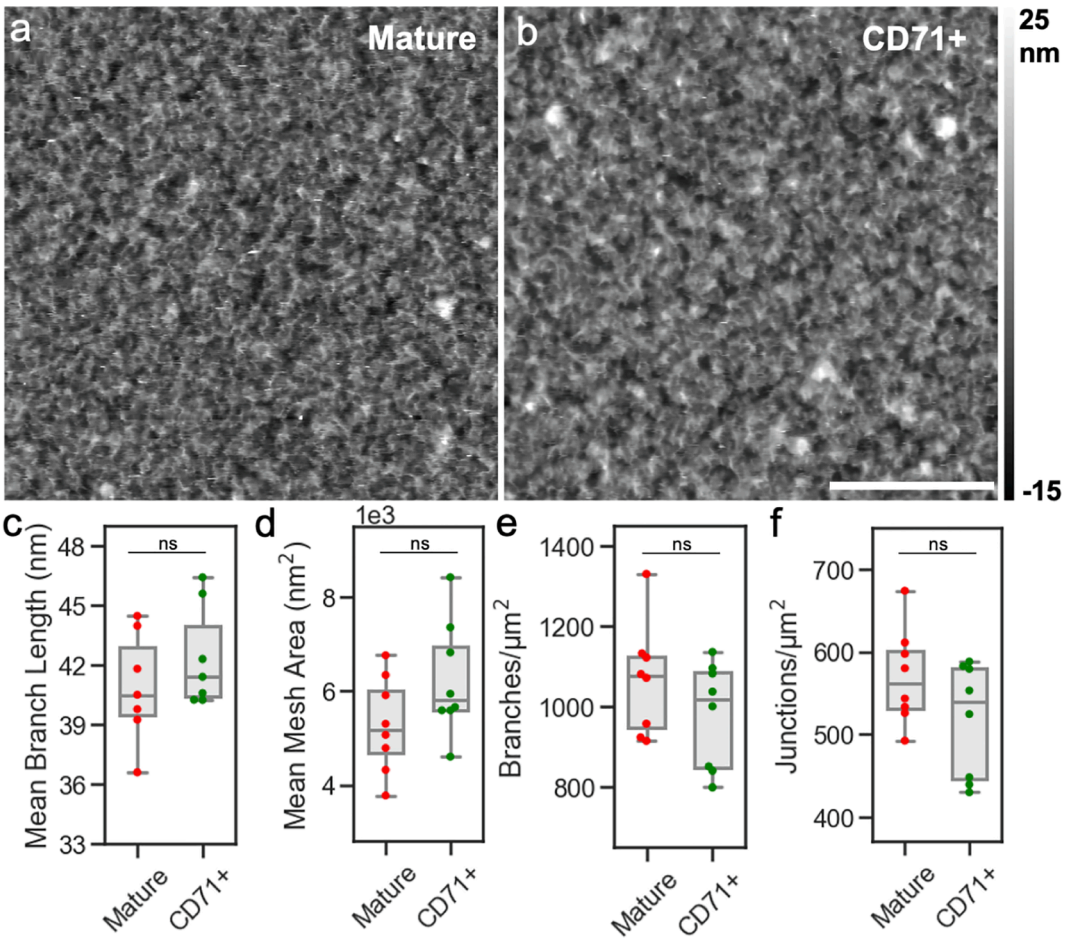

Fig. 5. AFM of hydrated membranes confirms the moderate shrinking of the skeletal meshwork as reticulocytes mature. (a, b) AFM images of hydrated sheared membranes from mature RBCs and CD71+ reticulocytes. The greyscale intensity represents the relative height within the sample in nm. (c–f) *Skan* statistics from SEM images pooled from 3 biological replicates (cord blood): mean junction-junction branch length (c) ($p = 0.3168$), mean mesh size (d) ($p = 0.1063$), branch density (e) ($p = 0.2204$), and junction density (f) ($p = 0.1267$) are shown.

using different sample preparations methods. Measurement of the network branch length has produced a range of results, depending on the technique, sample processing and the measurement method. Our SEM-based measurements of junction-junction branch length are in general agreement with those from cryo-TEM of mouse RBCs and AFM measurements of human RBCs (Nans et al., 2011; Swihart et al., 2001); however, it is worth noting that measurements of RBC membrane structures are heavily dependent on sample preparation procedures (Ohno et al., 1994; Takeuchi et al., 1998), and the branch structures observed in micrographs are assumed to be composites. We therefore refer to network branch length, rather than spectrin length, when referring to statistical measurements from image data.

Our SEM-based measurements of skeletal meshwork dimensions in dehydrated, gold coated specimens are slightly higher than those obtained from our AFM-based measurements of hydrated samples. It is likely that membrane structures are perturbed by the dehydration process even when using methods such as critical point drying. Nonetheless, a comparison of structures in the same state remains valid; and we observed an anticipated ~3.5% expansion of the meshwork branch length following osmotic swelling of mature RBCs.

Several studies suggest that reticulocytes have about 20% more surface area than mature RBCs (Killmann, 1964; Waugh et al., 1997). Our measurements suggest this difference is closer to 30% in volume and surface area, when only CD71+ reticulocytes are considered. Reticulocytes are also reported to have a higher shear modulus than mature RBCs (Malleret et al., 2013). The spectrin network is capable of undergoing significant and prolonged expansion (Discher et al., 1994) and it has been postulated that the skeletal network is stretched in reticulocytes, a conclusion supported by the observation that membrane vesiculation during reticulocyte maturation is spectrin-deficient (Ovchynnikova et al., 2018). The strain induced by expansion could also account for their reduced deformability compared to mature cells (Li et al., 2018; Namvar et al., 2021; Xie et al., 2006). However, quantitative proteomics has produced conflicting results on the relative amounts of skeletal proteins in mature cells compared with reticulocytes, with reports of less (Gautier et al., 2018; Liu et al., 2010) or more (Chu et al., 2018; Wilson et al., 2016) spectrin at maturity.

The skeletal meshwork of reticulocyte membranes has also been examined by different microscopy modalities. An AFM study reported that reticulocyte membranes have visibly larger mesh areas (Liu et al., 2003). We note, however, that these cells were not confirmed to be CD71+, and that the mean branch lengths for mature RBCs reported in this study were on the order of 160 nm, which is 3x greater than values found in this study. Such a substantially altered network may be a result of air-drying unfixed RBC membranes (Takeuchi et al., 1998). A more recent AFM study of CD71+ cells also measured network branch lengths, performing manual measurements with a sample size of <400 branches per type (Chu et al., 2018). This study reports a large difference in the network branch length, with ~17% longer connections in reticulocytes (Li et al., 2018). Again, this study used non-fixed samples that may have collapsed during air drying.

Here, we observed only a very moderate expansion of the skeletal

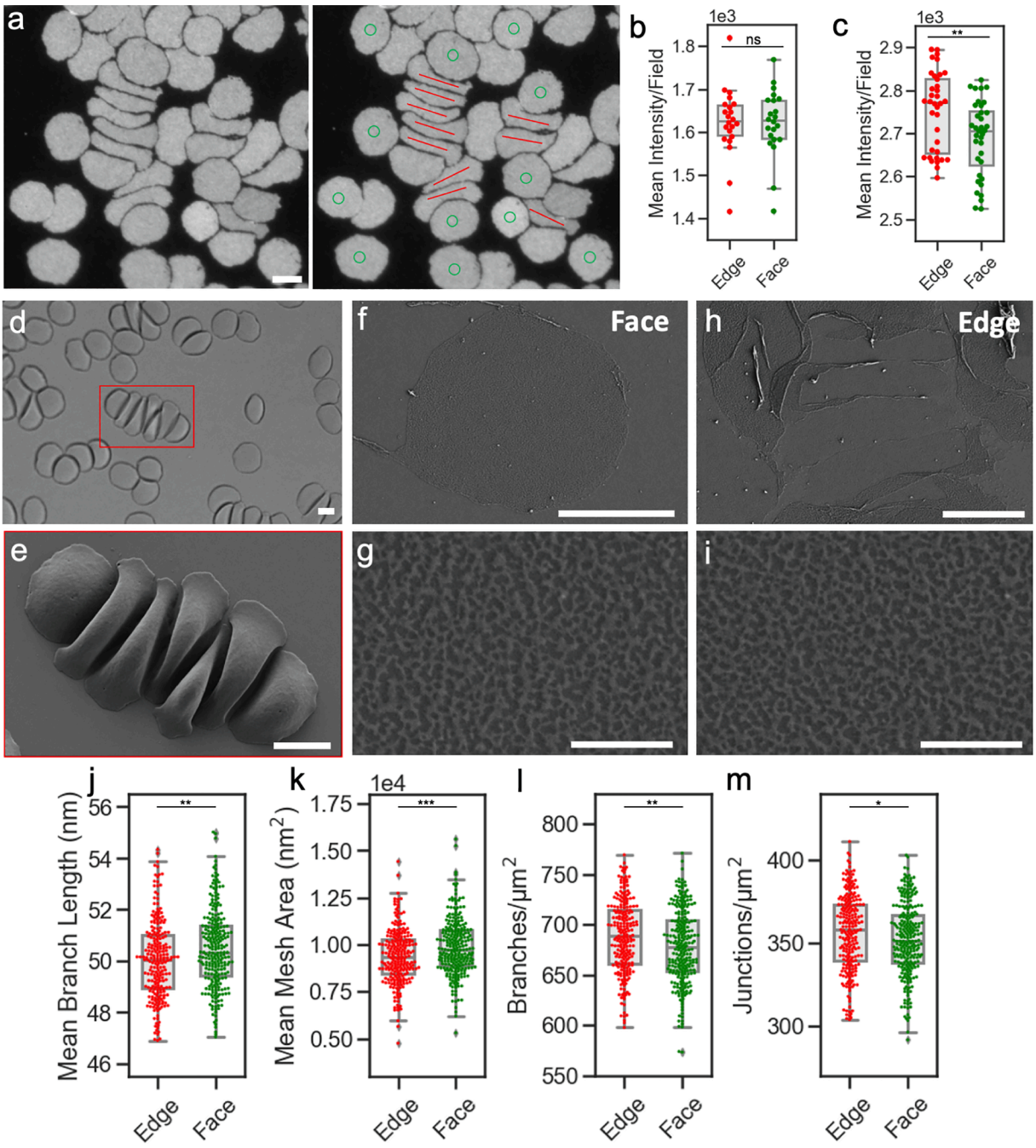

Fig. 6. Dimple regions of RBCs exhibit an expanded meshwork compared with the rim region. (a) Fluorescence microscopy images of sheared membranes labelled for spectrin with annotation denoting RBCs attached at the edge/rim (red lines) and face/dimple (green circles). (b, c) Intensity per area measurements were averaged per image field for spectrin (b) and band 4.1 (c). (d) Bright field optical imaging shows the cells attached before shearing and whole cells in the middle of rouleaux hold their edge-on alignment in whole cell SEM (e). (f–i) SEM of sheared membranes in face-on (f, g) and edge-on (h, i) orientations. Scale bars = 5 µm (a,d,e,f,h) and 500 nm (g,i). *Skan* analysis of junction-junction branch length (j), mean mesh area (k), junction density (l) and branch density (m). The mean values for images from 3 separate experiments are shown. Unpaired T-test: * = $p \leq 0.05$; ** = $p \leq 0.01$; *** = $p \leq 0.001$. (For interpretation of the references to colour in this figure legend, the reader is referred to the web version of this article.)

meshwork in CD71+ membranes, using SEM, and confirmed the finding using AFM of hydrated samples – the first time, to our knowledge, such measurements have been performed on reticulocyte membranes. Many thousands of automated measurements were needed to extract the small (2–4%) differences between reticulocytes and mature RBCs. We suggest that the use of preservative fixation and gentle dehydration may have helped preserve the membrane ultrastructure.

In contrast to the very limited changes in the physical meshwork, we observed larger changes in labelling of the skeletal and integral membrane components by immunofluorescence methods. For example, we observed an increase in density of labelling with spectrin (16%) and actin (21%) in mature RBCs compared with reticulocytes, as might be expected with a 20% loss of the lipid bilayer. This also corresponds well to the 13–18% decreased mesh area in mature RBCs as determined from SEM and AFM images.

Immunofluorescence analysis of ankyrin, dematin and Band 4.1, which are known to be associated with the junctional complexes pinning the spectrin-actin network to the plasma membrane (Fig. 3c), were

found to be approximately 15, 14 and 6% higher, respectively, in mature RBCs. This is consistent with the higher number of junctions (6–9%) measured in SEM and AFM images in membranes of mature RBCs. Unexpectedly, adducin, another protein known to facilitated linkages between the spectrin-actin network and junctional complexes, was found to have a higher density in reticulocytes. It is possible that a higher level of adducin might help compensate for the increased strain introduced by having fewer connections within the network, but this remains a question for further study.

The dynamic nature of the RBC membrane components is increasingly recognised (Gokhin and Fowler, 2016; Kuck et al., 2020). For example, spectrin tetramers can self-associate to form higher-order oligomers (Nans et al., 2011; Ursitti and Wade, 1993). Our findings suggest a sparser network in reticulocytes but only a very moderate increase in the mean branch length. If negligible spectrin is lost during maturation, our results suggest that the spectrin-actin network moves to higher order spectrin configurations during cell maturation, thereby increasing the density of the network without significantly changing the network branch length. A schematic for how this change in branch density may appear on a molecular scale is depicted in Fig. 7, taking into account the component densities measured by microscopy.

The characteristic biconcave resting shape of the mature RBC is intriguing; but until now the question as to whether there are physical differences in the organisation of the skeletal meshwork in the edge region vs that of the dimple has not been directly addressed. There is some debate in the RBC modelling literature as to the resting state of the RBC, i.e., whether the stress-free geometry is spherical, biconcave or some other shape (Li et al., 2007; Peng et al., 2014); however models developed so far have not taken into account any changes in membrane composition over the cell surface.

We directly analysed the membrane skeleton in RBCs oriented edge-on compared to those oriented face-on, and found a subtle yet measurable difference between the two orientations. This is consistent with the suggestion that the previously demonstrated presence of shape-memory (Fischer, 2004) and the preferential edge-on orientation of RBCs in a centrifugal field are due to real differences in RBC membrane protein organisation (Hoffman, 2018). Our results suggest that this difference arises from a 1–2% increase in the number of junctions in the edge region. It is worth noting that this small difference is likely to be functionally significant, considering that hypo-osmotic swelling, almost to the point of cell lysis, only introduces a 6% difference in junction density. The labelling profile of band 4.1 is consistent with the increase in junction density and decrease in mean branch length measured from SEM images.

We note that there is no change in density for the spectrin fluorescence signal associated with the increased junction density. We suggest that may be due to partial re-arrangement of spectrin configurations along the edge, as depicted in Fig. 7. An accompanying 4–5% decrease in mesh size in rim membranes supports this suggestion. We also note that mature RBCs, which exbibit a denser network, are more flexible than their reticulocyte counterparts. Accordingly, our results suggest that the RBC's rim will be slightly more deformable than the face region.

Overall, these results challenge the current idea that skeletal branch lengths are markedly expanded in reticulocyte membranes compared with mature RBC membranes. The methods developed in this work will be useful in studying RBCs possessing mutations in membrane skeleton components and in the study of RBC membranes from patients with haemoglobinopathies such as HbSS. Our results will inform future modelling studies of RBC membrane dynamics, and aid in the understanding of how these cells maintain their shape and perform their functions at different stages of their lifespan.

Conclusions

Correlative and multimodal microscopy-based analyses show that the reticulocyte membrane skeleton is much denser than suggested by previous studies. It undergoes only a small (<4%) contraction in the network branch length upon maturation of reticulocytes to erythrocytes. We propose that the large (up to 30%) volume and surface area differences exhibited by reticulocytes are underpinned by a shift in spectrin conformation from tetramers to higher order oligomers.

We also examined the membranes of RBCs oriented either edge-on or face-on, finding a subtle but consistent difference in the junctional density. Rim-oriented membranes show a 1–2% greater density compared to dimple-orientated membranes, suggesting that adopting the biconcave disc shape relies on inhomogeneity within the RBC membrane skeleton and dynamic changes in the spectrin self-association state.

CRediT authorship contribution statement

Adam J. Blanch: Conceptualization, Methodology, Investigation, Writing - original draft, Writing - review & editing. **Juan Nunez-Iglesias:** Software. **Arman Namvar:** Methodology, Investigation. **Sebastien Menant:** Methodology, Resources. **Oliver Looker:** Methodology. **Vijay Rajagopal:** Supervision, Writing - review & editing. **Wai-Hong Tham:** Resources, Writing - review & editing. **Leann Tilley:** Conceptualization, Writing - review & editing, Supervision. **Matthew W.A Dixon:** Conceptualization, Methodology, Writing - review & editing, Supervision.

Declaration of Competing Interest

The authors declare that they have no known competing financial

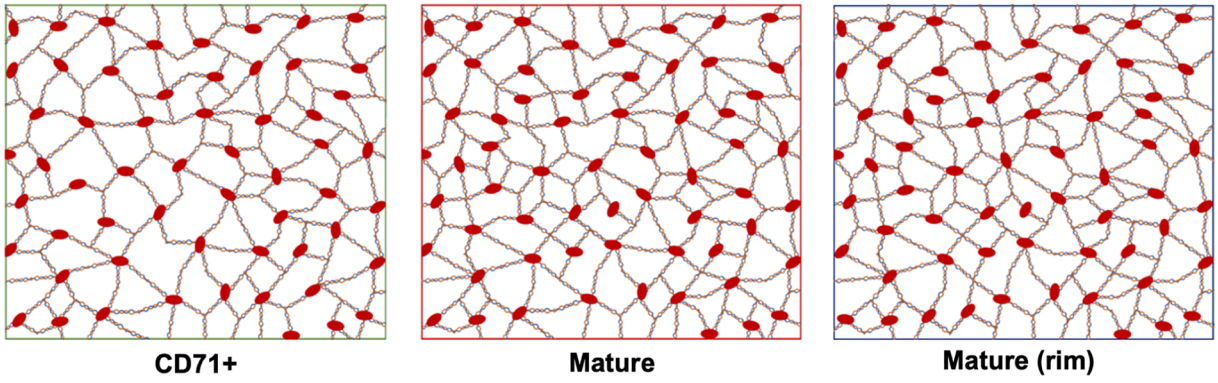

Fig. 7. Basic model of reticulocyte, mature and mature rim RBC meshworks. Schematic models of the RBC meshwork with spectrin unit, band 4.1 junctional unit (red ovals), branch and junction densities depicted to approximate microscopy measurements (Fig. S6). (For interpretation of the references to colour in this figure legend, the reader is referred to the web version of this article.)

interests or personal relationships that could have appeared to influence the work reported in this paper.

Acknowledgements

The authors thank the Australian Red Cross Blood Service and the BDMI Cord Blood Bank. Fluorescence microscopy was performed at the Biological Optical Microscopy Platform and electron microscopy was carried out at the Ian Holmes Imaging Centre at Bio21, the University of Melbourne (www.microscopy.unimelb.edu.au). AFM was performed at the Materials Characterisation and Fabrication Platform (MCFP), The University of Melbourne. We would like to thank Sebastien Menant, Li-Jin Chan and Sravya Keremane for their support in reticulocyte purification. LT is a Georgina Sweet, Australian Research Council Laureate Fellow (FL150100106) (http://www.arc.gov.au). W.-H.T. is a Howard Hughes Medical Institute-Wellcome Trust International Research Scholar (208693/Z/17/Z) and supported by National Health and Medical Research Council of Australia (GNT1143187, GNT1160042, GNT1160042, GNT1154937). MWAD and LT thank the National Health and Medical Research Council (GNT1098992) (https://www.nhmrc.gov.au) for funding support. AB received support from a UoM ECR Grant.

Appendix A. Supplementary data

Supplementary data to this article can be found online at https://doi.org/10.1016/j.yjsbx.2021.100056.

References

Alimohamadi, H., Smith, A.S., Nowak, R.B., Fowler, V.M., Rangamani, P., 2020. Non-uniform distribution of myosin-mediated forces governs red blood cell membrane curvature through tension modulation. PLOS Comput. Biol. 16 e1007890.
An, X., Mohandas, N., 2008. Disorders of red cell membrane. Br. J. Haematol. 141, 367–375.
Basu, A., Harper, S., Pesciotta, E.N., Speicher, K.D., Chakrabarti, A., Speicher, D.W., 2015. Proteome analysis of the triton-insoluble erythrocyte membrane skeleton. J. Proteomics 128, 298–305.
Byers, T.J., Branton, D., 1985. Visualization of the protein associations in the erythrocyte membrane skeleton. Proc. Natl. Acad. Sci. 82 (18), 6153–6157.
Chasis, J.A., Prenant, M., Leung, A., Mohandas, N., 1989. Membrane assembly and remodeling during reticulocyte maturation. Blood 74, 1112–1120.
Chu, T.T.T., Sinha, A., Malleret, B., Suwanarusk, R., Park, J.E., Naidu, R., Das, R., Dutta, B., Ong, S.T., Verma, N.K., Chan, J.K., Nosten, F., Rénia, L., Sze, S.K., Russell, B., Chandramohanadas, R., 2018. Quantitative mass spectrometry of human reticulocytes reveal proteome-wide modifications during maturation. Br. J. Haematol. 180 (1), 118–133.
Come, S.E., Shohet, S.B., Robinson, S.H., 1972. Surface remodelling of reticulocytes produced in response to erythroid stress. Nat. New Biol. 236 (66), 157–158.
Discher, D.E., Mohandas, N., Evans, E.A., 1994. Molecular maps of red cell deformation: hidden elasticity and in situ connectivity. Science 266 (5187), 1032–1035.
Fischer, T.M., 2004. Shape memory of human red blood cells. Biophys. J . 86 (5), 3304–3313.
Fowler, V.M., 2013. Chapter two - the human erythrocyte plasma membrane: a Rosetta Stone for decoding membrane-cytoskeleton structure. In: Vann, B. (Ed.), Current Topics in Membranes. Academic Press, pp. 39–88.
Gautier, E.-F., Leduc, M., Cochet, S., Bailly, K., Lacombe, C., Mohandas, N., Guillonneau, F., El Nemer, W., Mayeux, P., 2018. Absolute proteome quantification of highly purified populations of circulating reticulocytes and mature erythrocytes. Blood Adv. 2, 2646–2657.
Gifford, S.C., Derganc, J., Shevkoplyas, S.S., Yoshida, T., Bitensky, M.W., 2006. A detailed study of time-dependent changes in human red blood cells: from reticulocyte maturation to erythrocyte senescence. Br. J. Haematol. 135 (3), 395–404.
Gokhin, D.S., Fowler, V.M., 2016. Feisty filaments: actin dynamics in the red blood cell membrane skeleton. Curr. Opin. Hematol. 23 (3), 206–214.
Hoffman, J.F., 2016. Biconcave shape of human red-blood-cell ghosts relies on density differences between the rim and dimple of the ghost's plasma membrane. Proc. Natl. Acad. Sci. 113 (51), 14847–14851.
Hoffman, J.F., 2018. Evidence that asymmetry of the membrane/cytoskeletal complex in human red blood cell ghosts is responsible for their biconcave shape. Proc. Natl. Acad. Sci.
Killmann, S.-A., 1964. On the size of normal human reticulocytes. Acta Med. Scand. 176, 529–533.
Kuck, L., Peart, J.N., Simmonds, M.J., 2020. Active modulation of human erythrocyte mechanics. Am. J. Physiol. -Cell Physiol. 319 (2), C250–C257.
Li, H.e., Yang, J., Chu, T.T., Naidu, R., Lu, L.u., Chandramohanadas, R., Dao, M., Karniadakis, G.E., 2018. Cytoskeleton remodeling induces membrane stiffness and stability changes of maturing reticulocytes. Biophys. J . 114 (8), 2014–2023.
Li, J., Lykotrafitis, G., Dao, M., Suresh, S., 2007. Cytoskeletal dynamics of human erythrocyte. Proc. Natl. Acad. Sci. 104 (12), 4937–4942.
Liu, F., Burgess, J., Mizukami, H., Ostafin, A., 2003. Sample preparation and imaging of erythrocyte cytoskeleton with the atomic force microscopy. Cell Biochem. Biophys. 38 (3), 251–270.
Liu, J., Guo, X., Mohandas, N., Chasis, J.A., An, X., 2010. Membrane remodeling during reticulocyte maturation. Blood 115, 2021–2027.
Liu, S.C., Derick, L.H., Palek, J., 1987. Visualization of the hexagonal lattice in the erythrocyte membrane skeleton. J. Cell Biol. 104, 527–536.
Looker, O., Blanch, A.J., Liu, B., Nunez-Iglesias, J., McMillan, P.J., Tilley, L., Dixon, M.W. A., 2019. The knob protein KAHRP assembles into a ring-shaped structure that underpins virulence complex assembly. PLoS Pathog 15.
Lux, S.E., 2016. Anatomy of the red cell membrane skeleton: unanswered questions. Blood 127, 187.
Malleret, B., Xu, F., Mohandas, N., Suwanarusk, R., Chu, C., Leite, J.A., Low, K., Turner, C., Sriprawat, K., Zhang, R., Bertrand, O., Colin, Y., Costa, F.T.M., Ong, C.N., Ng, M.L., Lim, C.T., Nosten, F., Rénia, L., Russell, B., 2013. Significant biochemical, biophysical and metabolic diversity in circulating human cord blood reticulocytes. PLoS ONE 8.
Mankelow, T.J., Satchwell, T.J., Burton, N.M., 2012. Refined views of multi-protein complexes in the erythrocyte membrane. Blood Cells Mol. Dis. 49 (1), 1–10.
Minetti, G., Achilli, C., Perotti, C., Ciana, A., 2018. Continuous change in membrane and membrane-skeleton organization during development from proerythroblast to senescent red blood cell. Front. Physiol. 9, 286.
Mohandas, N., Gallagher, P.G., 2008. Red cell membrane: past, present, and future. Blood 112, 3939.
Namvar, A., Blanch, A.J., Dixon, M.W., Carmo, O.M.S., Liu, B., Tiash, S., Looker, O., Andrew, D., Chan, L.-J., Tham, W.-H., Lee, P.V.S., Rajagopal, V., Tilley, L., 2021. Surface area-to-volume ratio, not cellular viscoelasticity, is the major determinant of red blood cell traversal through small channels. Cell. Microbiol. 23 (1) https://doi.org/10.1111/cmi.v23.110.1111/cmi.13270.
Nans, A., Mohandas, N., Stokes, D., 2011. Native ultrastructure of the red cell cytoskeleton by cryo-electron tomography. Biophys. J . 101 (10), 2341–2350.
Nunez-Iglesias, J., Blanch, A.J., Looker, O., Dixon, M.W., Tilley, L., 2018. A new Python library to analyse skeleton images confirms malaria parasite remodelling of the red blood cell membrane skeleton. PeerJ 6, e4312.
Ohno, S., 1992. An ultrastructural study of the cytoplasmic aspects of erythrocyte membranes by a quick-freezing and deep-etching method. J. Anat. 180, 315–320.
Ohno, S., Terada, N., Fujii, Y., Ueda, H., 1994. Membrane skeleton in fresh unfixed erythrocytes as revealed by a rapid-freezing and deep-etching method. J. Anat. 185, 415–420.
Ovchynnikova, E., Aglialoro, F., von Lindern, M., van den Akker, E., 2018. The shape shifting story of reticulocyte maturation. Front. Physiol. 9, 829.
Pan, L., Yan, R., Li, W., Xu, K., 2018. Super-resolution microscopy reveals the native ultrastructure of the erythrocyte cytoskeleton. Cell Rep. 22, 1151–1158.
Peng, Z., Mashayekh, A., Zhu, Q., 2014. Erythrocyte responses in low-shear-rate flows: effects of non-biconcave stress-free state in the cytoskeleton. J. Fluid Mech. 742, 96–118.
Salomao, M., Zhang, X., Yang, Y., Lee, S., Hartwig, J.H., Chasis, J.A., Mohandas, N., An, X., 2008. Protein 4.1R-dependent multiprotein complex: new insights into the structural organization of the red blood cell membrane. Proc. Natl. Acad. Sci. 105, 8026–8031.
Smith, A.S., Nowak, R.B., Zhou, S., Giannetto, M., Gokhin, D.S., Papoin, J., Ghiran, I.C., Blanc, L., Wan, J., Fowler, V.M., 2018. Myosin IIA interacts with the spectrin-actin membrane skeleton to control red blood cell membrane curvature and deformability. Proc. Natl. Acad. Sci. 115, E4377.
Swihart, A.H., Mikrut, J.M., Ketterson, J.B., Macdonald, R.C., 2001. Atomic force microscopy of the erythrocyte membrane skeleton. J. Microsc. 204, 212–225.
Takeuchi, M., Miyamoto, H., Sako, Y., Komizu, H., Kusumi, A., 1998. Structure of the erythrocyte membrane skeleton as observed by atomic force microscopy. Biophys. J . 74, 2171–2183.
Ursitti, J.A., Wade, J.B., 1993. Ultrastructure and immunocytochemistry of the isolated human erythrocyte membrane skeleton. Cell Motil. Cytoskelet. 25, 30–42.
Waugh, R.E., Mantalaris, A., Bauserman, R.G., Hwang, W.C., Wu, J.H., 2001. Membrane instability in late-stage erythropoiesis. Blood 97, 1869–1875.
Waugh, R.E., McKenney, J.B., Bauserman, R.G., Brooks, D.M., Valeri, C.R., Snyder, L.M., 1997. Surface area and volume changes during maturation of reticulocytes in the circulation of the baboon. J. Lab. Clin. Med. 129, 527–535.
Wilson, M.C., Trakarnsanga, K., Heesom, K.J., Cogan, N., Green, C., Toye, A.M., Parsons, S.F., Anstee, D.J., Frayne, J., 2016. Comparison of the proteome of adult and cord erythroid cells, and changes in the proteome following reticulocyte maturation. Mol. Cell. Proteomics 15, 1938–1946.
Xie, L., Jiang, Y., Yao, W., Gu, L., Sun, D., Ka, W., Wen, Z., Chien, S., 2006. Studies on the biomechanical properties of maturing reticulocytes. J. Biomech. 39, 530–535.